Ambient Noise Cross-Correlation Study of Menengai Caldera: Geothermal Prospect in the Central Kenya Dome

Ezer Patlan[1], Antony Wamalwa[2], Galen Kaip[1], and Aaron A. Velasco[1]

[1]University of Texas at El Paso, El Paso TX
[2]Geothermal Development Company, Nairobi, Kenya
epatlan@miners.utep.edu

Keywords

Earthquakes, ambient noise cross-correlation, automatic frequency time analysis, and hydrothermal

ABSTRACT

The Geothermal Development Company (GDC) and the University of Texas at El Paso (UTEP) have deployed fourteen seismic stations around the Menengai geothermal field along the Kenya rift system to monitor the seismicity around the host volcano to help identify active faults and fracture systems that may contain hydrothermal fluids and favorable drilling targets. Double difference relocation was used to locate events and to image faulting the margin of the caldera. We then apply an ambient noise tomography approach to image the Earth's medium. Specifically, we cut the waveform data at single seismic station for every one hour in the vertical component and preprocess the noise using 1-bit normalization to eliminate the earthquake noise signal and the instrumentation irregularities. We apply spectral whitening to reduce the seismic amplitude. The cross-correlation between two different seismic stations were used to retrieve the Green's function. We used Automatic Frequency time analysis (AFTAN) and phase match filtering analysis (MTA) in order to approximate the group velocities. Finally, we will then use the group velocity curves in a tomography algorithm to identify the hydrothermal reservoir zone.

1. Introduction

Geophysical studies over geothermal fields can provide fundamental information about the subsurface structures and processes that are key to siting high producing wells to tap the resource (e.g., Simiyu and Keller, 2000; Simiyu, 2000, 2009; Wilson et al., 2003). Although resistivity and potential field (gravity and magnetic) methods have been used to identify faults and fractures and intrusions (e.g. Árnason et al., 2010; Newman et al., 2008; Wamalwa et al., 2011), the techniques can also identify the depth range of active faults that can lead to fluid channels in an inactive fault. Micro-earthquake studies can help in identifying active faults from accurate event locations, and thus be used to infer fluid movement. Simiyu and Keller (2001) identify micro fault system ranging from 0 to 8 km depth using microseismic relocation. This will allow us to locate the brittle-ductile transition zone in order to identify porosity changes. With this information, we can aid where to target drilling of the geothermal reservoir. Hence, the main goal of this project is to collect and analyze seismic data in order to identify the fluid pathways and zones with fluid phase change.

In order to accomplish these goals, the Geothermal Development Company (GDC) and the Department of Geological Sciences at the University of Texas at El Paso (UTEP) installed a total of fourteen seismometers around the Menengai region since March 2011. Seven instruments (Phase 1) were installed in March

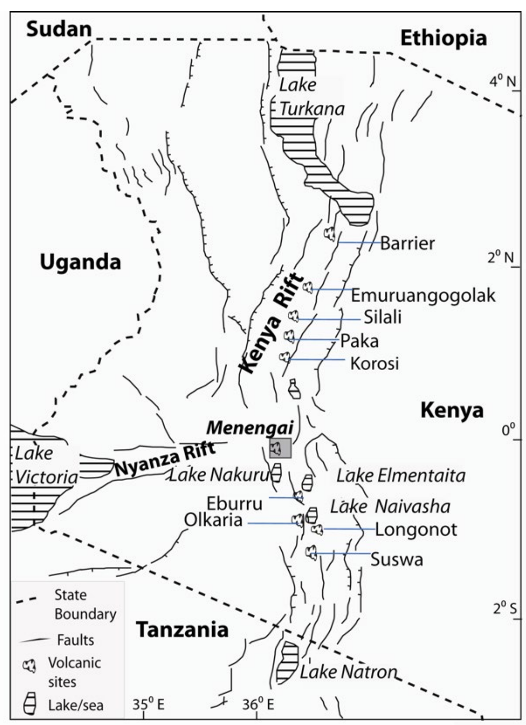

Figure 1. Map of Kenya rift showing the Menengai Caldera along with various volcanoes in the region.

and the other seven (Phase 2) in August 2011. We deployed three types of sensors including broadband Guralp 40T, intermediate Guralp 3T, and short period sensors HS10. Each sensor was placed in a shallow vault (1m in depth). Here, we present the initial results of eleven months of recording from Phase 1 and 2.

1.1 Menengai Geology and Previous Geophysical Studies

The Menengai volcano is located at the intra-continental crustal triple junction north of the Nakuru-Naivasha basin where the Nyanza rift joins the Kenya rift (Figure 1). The Menengai region is dominated by a central volcano with a large caldera of about 12 km in diameter.

The caldera has steep sides of up to 300 m high where old shield lavas are exposed. Pyroclastics and tuffs cover the rest of the area outside the caldera. The volcanic suite comprises phonolites, trachyphonolites and trachytes. The source of the pyroclastics evolved from the subsequent eruptions that led to the formation of the large caldera.

Previous seismic studies have imaged a high velocity body beneath the Menengai volcano (Simiyu and Keller, 2000). An integrated study that combined seismic and gravity data for the southern section of the rift (Simiyu and Keller, 2001) relocated swarms of micro-events ranging from 0 to 8 km depth and showed a distribution of high heat based on the seismicity changes with depth in Olkaria, Kenya. Recent resistivity studies (Wamalwa et al., 2011, in review) have imaged a conductive zone at about 6 km deep below the surface, which was interpreted as molten rocks.

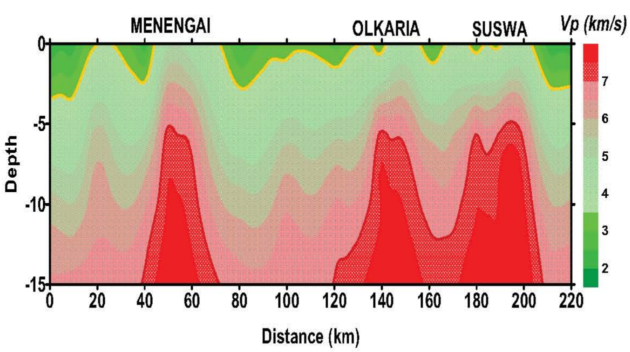

Figure 2. Seismic velocity models along the rift axis showing high Velocity zones beneath Menengai Olkaria and Suswa Volcanic centers (Simiyu and Keller, 2000).

A similar interpretation from micro-earthquake analysis (Simiyu, 2009) observed that most of the events within the caldera were restricted to the upper 6 km depth indicating a brittle-ductile transition zones at this depth that suggest the presence of a hot magma material. Our study is aimed to further analyze micro-earthquakes in this region by precisely locating events using a double difference approach (HypoDD) and identifying high temperature fluid filled zones that will be favorable for production wells with high yield.

2. Data and Processing

Phase 1 of the seismic station deployment comprised of seven stations (Table 1). Our priority for selecting sites was to adequately cover the Caldera area, and place sites in secure locations. The data presented here were recorded from this station from March to July 2011. Phase 2 of the seismic station deployment were recorded outside the rim of the caldera and deployed in August 2011. We deployed a suite of instruments, including broadband, intermediate, and short period sensors that will allow us to locate earthquakes and apply a suite of techniques to identify source processes of volcanic earthquakes, including long period events that can potentially identify fluid movement.

Table 1. Site locations for Phase 1 & 2.

Station Code	Lat. (°)	Lon. (°)	Elevation (m)	Sensor	Description
			Phase 1		
MNC1	-0.19375	36.08299	1867	HS10	Caldera
BHT	-0.14252	36.15708	2119	3T	School House
LWHS	-0.2222	36.1767	2068	3T	School
RGO	-0.15607	36.04936	1948	40T	School
TOR1	-0.17776	36.00686	1942	HS10	Homestead
KIMU	-0.26657	36.02494	1941	3T	School
VWP	-0.25946	36.09253	2106	40T	Homestead
			Phase 2		
NGSS	-0.1822	36.2446	2730	40T	School
DIGR	-0.0964	35.9846	1700	3T	Homestead
SLS	-0.0999	36.1278	1869	40T	School
NDG	-0.1064	36.0594	2068	40T	School
MNP	-0.2179	35.9466	1991	3T	School
BLS	-0.1145	36.1599	2173	40T	School

We quality check the continuously recorded data by reviewing all data logs, checking for time gaps and timing error. Although we had excellent recovery rates for the data, we find 1 s time jumps on three stations that we corrected.

3. Methodology

3.1 Double Difference Earthquake Relocation

Once we have archived and checked for quality and using the BRTT Antelope Software, we performed automatic detections using a short-term and long-term average (STA/LTA) detection algorithm to identify possible seismic arrivals. We use different filters and detection parameters to search for local events using: 1) a high pass filter at 5 Hz to highlight local impulsive earthquakes (STA of 1 s; LTA of 10 s); 2) a high pass filter at 5 Hz to highlight local emergent (tremor) events (STA of 60 s; LTA of 600 s); and 3) a low pass filter at 20 s to highlight possible long-period events (STA of 60 s; LTA of 600 s).

After the automatic detections are made, we associate arrivals to possible hypothetical events, and develop an automated catalog of earthquakes. The catalog includes local events, which we review manually. During review, we re-pick *P* waves and relocate the events using a standard approach to develop a new, local catalog that serves as the foundation for our double difference approach.

In order to relocate earthquakes, the seismic network must surround the seismic sources. To determine if an earthquakes lies within the network of stations (and can be located with high confidence), we calculate the maximum station-event azimuth, called azimuthal gap, using our catalog. The azimuthal gap is defined as the maximum angle between event-station pairs; and for an event to be within our networks, the azimuthal gap must be less than 180°. To accomplish high precision earthquake locations, we applied the double difference earthquake location method (Waldhauser and Ellsworth, 2000) at Menengai, Caldera. The double difference earthquake location method (hypoDD) uses two important attributes that make earthquake locations high precision: high precision *P* wave arrival times and event clusters to remove the dependence on the velocity structure. We manually picked the *P* arrival time for every event previously determined and then compute a cross-correlated time pick for all events and stations.

3.2 Ambient Noise Tomography

We apply an ambient noise tomography technique that has been previously developed (Bensen et al., 2007, 2008 and Lin et al., 2008). We remove the instrumentation response from the Guralp 40T, Guralp 3T, Trillium Compact, Streckeisen STS-1V/VBB, Streckeisen STS-2 G1, and HS10 sensors, using band-pass filters appropriate for each station pair. We remove the earthquake signals by applying a one-bit normalization, which generates a data stream composed only of the values 1 and -1, retaining only the sign and disregarding the amplitude of the signal completely (Bensen et al., 2007). Spectral whitening is then performed to reduce the seismic amplitude and/or to flatten the spectral over the entire period band (Bensen et al., 2007; Yang et al., 2011; Yang, Shen, and Ritzwoller, 2011). We retrieve the Green's function by cross-correlating the normalized waveforms between two seismic stations in one hour increments, and stacking in 3-month bins to account for seasonal variability and estimate the group velocity uncertainties (Campillo and Paul 2003; Nicolson et al., 2012).

Frequency time analysis done by Herrmann and Ammon (2004) and Levshin, Pisarenko, and Pogrebinsky (1972) is used to measure the dispersion curves of the Rayleigh waves. The group velocity is the velocity at which the energy-packet travels while the phase velocity describes the velocity of a phase at a given frequency. Both velocities are sensitive to the structure of the rocks through which the surface waves travel.

4. Preliminary Results

4.1 Double Difference Earthquake Relocation

For the initial, automated locations, we use the Antelope software package that automatically routine detected the *P* arrival time (Figure 3). We manually re-pick the *P*-wave and relocate the hypocenter using Antelope and HypoDD. Figure 3 shows the initial grid locations from March 2011 to March 2012, which then must be relocated to obtain the preliminary locations that we use for the double difference approach.

Table 2 shows the parameters that were used to link similar *P*-phase travel time events (using ph2dt) and produce a travel time catalog of event pairs. In order to evaluate the location of the events, a 1-D velocity model from Simuyi and Keller, 2000 is applied in the inversion as initial model. Figure 4 shows our preliminary double difference locations. Note the algorithm has removed a majority of our events, and we will explore the results further to guarantee that we ontain the most events possible.

Once we have determined a location, we approximate the local magnitude (M_L) using the distance between the station and event

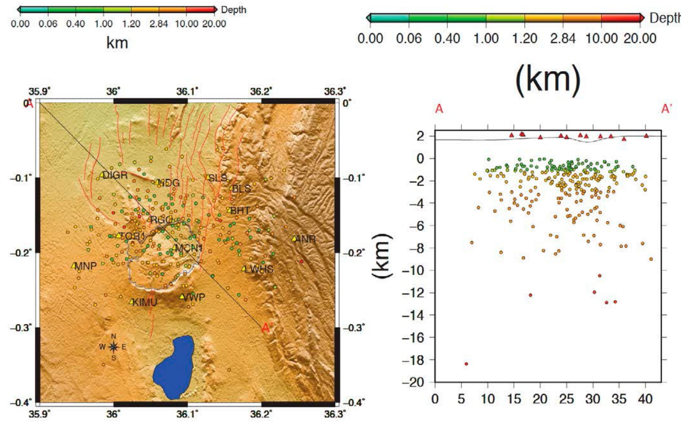

Figure 3. Shows 14 seismic stations (red triangles) deploy in Menengai Caldera. From March 2011 to March 2012, the preliminary local events (color circles) are located north and east-west providence of Menengai caldera.

(D) and the maximum amplitude (*A*) of the event:

$$M_L = \log_{10}(A) + 2.76\log_{10}(\Delta) - 2.48 \quad (1)$$

We remove the instrumentation response and apply a Wood Anderson instrument filter to the seismograph; the local magnitude can be approximated using equation 1.

We believe in Figure 4 from October through December 2011 Menengai has been active by the number of events per Julian day.

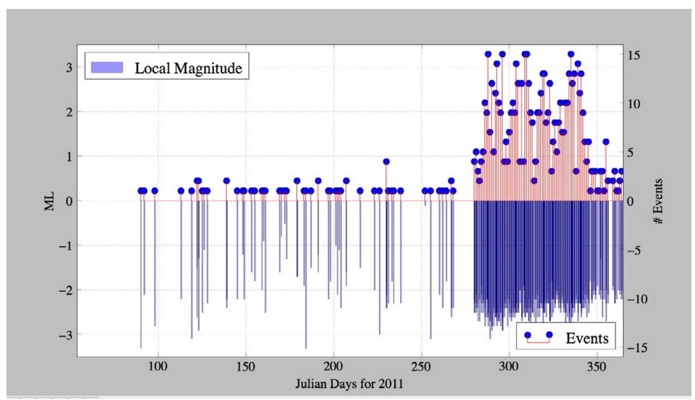

Figure 4. Shows the number of events per Julian day from April through December 2011. From the left y-axis in a blue line shows the local magnitude. From the right y-axis shows the number of events in blue circles that had relocated per Julian day.

The intensity of the events are micro magnitude that our cause by hydrothermal pockets within Menengai. To understand the cluster of events we proposed to determine the characteristics of the brittle-ductile transition zone, we propose the Power Spectral Density (PDS) approach that can be used along with size of the event (local magnitude) to identify a volcanic tectonic, long-period, hybrid, or tremor that helps us classified a hot springs, fumaroles and hydrothermal system (Chouet, 1996).

Table 2. Parameters used to generate network of delay time links from phase pick data (see Waldhauser, 2001 for parameter description).

MIN WGH	MAX DIST	MAX SEP	MAX NGH	MIN LNK	MIN OBS	MAX OBS
0.001	60	10	10	4	4	100

4.2 Ambient Noise Tomography

Figure 5 shows the ray coverage from regional to local network. We plan to approximate the group velocities using the regional network and for the phase velocities we will use the local network. In order to retrieve the group and phase velocities, we retrieve the Green's Function in Figure 6 by preprocessing the noise using normalization and spectral whiten in order to approximate the group velocity using Frequency time analysis by Herrmann and Ammon (2004) and Levshin, Pisarenko, and Pogrebinsky (1972) show in Figure 7. Figure 6 shows the stacked cross correlation of LSZ and VWP seismic station. We filter four band-pass filters at LSZ and VWP ranging from 10s – 25s to analyze the Green's function since each station has a difference sensor. For this application, the Streckeisen STS-1H/VBB sensor (LSZ) has a frequency range from 2s – 120s while the 40T sensor (VWP) has a frequency range from 2s – 30s. After analyzing the ambient noise cross-correlation, we apply Automatic Frequency Time Analysis (AFTAN) to approximate the group velocities show Figure 7 and 8.

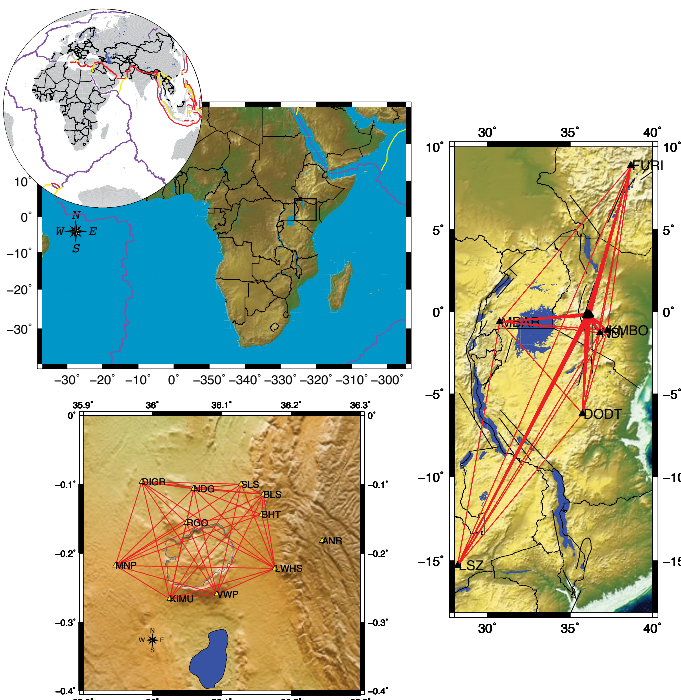

Figure 5. Top Left: Map view where our study area is located. Top Right: Show the AF, II and IU network that covers Ethiopia, Kenya, Uganda, Tanzania, and Zambia. Southwest of Kenya the Menengai network is located. Bottom Left: Zoom in to the Menengai network showing the ray coverage within Menengai Caldera.

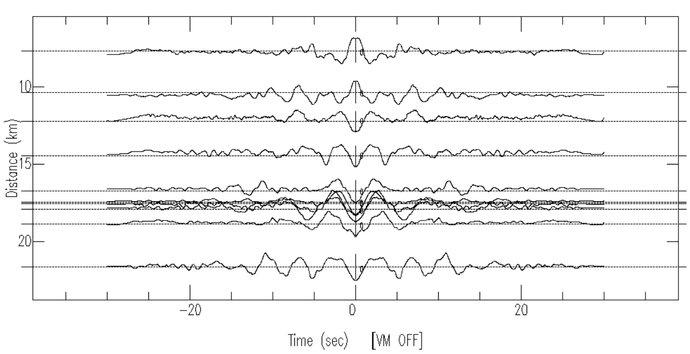

Figure 6. Ten month cross-correlation from April 2011 VWP stations and others stations filtered between periods of 5Hz – 10s. Clear surface wave signals appear in the cross-correlation.

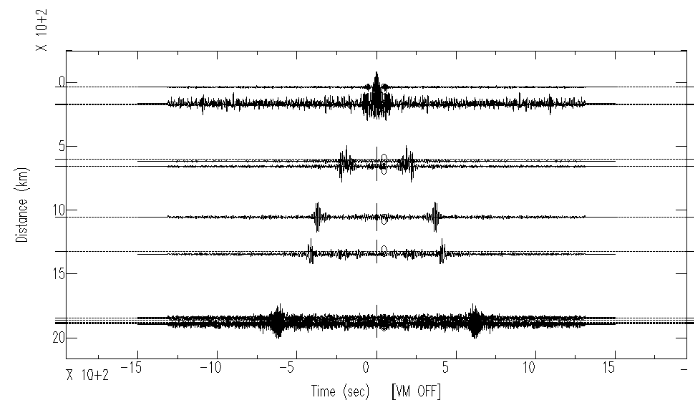

Figure 7. Ten month cross-correlation from April 2011 between the LSZ and MNP stations and others stations filtered between periods of 10s – 25s. Clear surface wave signals appear in the cross-correlation.

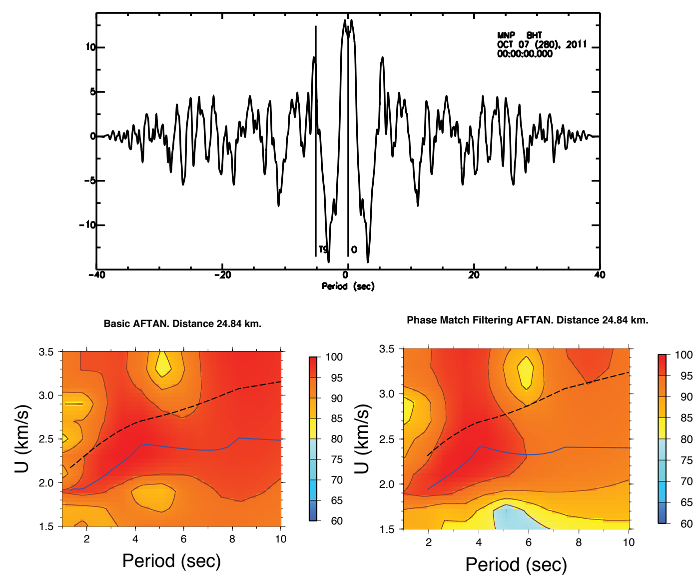

Figure 8. This is the local Rayleigh-wave Green's function. Top: Shows the ambient noise cross correlation between MNP and BHT seismic station with a band pass filter range from 5Hz-10s. Bottom Left: Basic Automatic Frequency Time Analysis (AFTAN). The blue dispersion curve is the observed and the black dash dispersion curve is the predicted. Bottom Right: Phase Matching Filtering is applied to the AFTAN. The color-coded map from blue to red is the amplitude dB. The x-axis represent the time frame in seconds and the y-axis represent the group velocity.

For the Menengai network, figure 6 shows a range of local distances from the Menengai network of 4 km to 25 km displaying the Rayleigh-wave Green's functions. Figure 8 on the top shows the time domain of the Green's functions and at the bottom we calculate the group velocities using the FTAN and phase Match Filtering Analysis (MTA) using BHT and VWP station. We conclude that shorter distance from 4 km to 10 km would not display the surface wave. For the regional network show figure 5, figure 7 shows

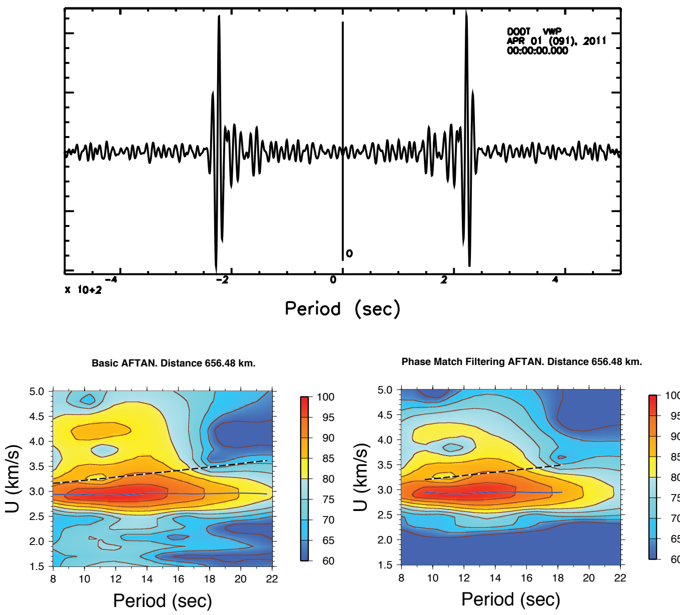

Figure 9. This is the regional Rayleigh-wave Green's function. Top: Shows the ambient noise cross correlation between DODT and VWP seismic station with a band pass filter range from 10-25s. Bottom Left: Basic Automatic Frequency Time Analysis (AFTAN). The blue dispersion curve is the observed and the black dash dispersion curve is the predicted. Bottom Right: Phase Matching Filtering is applied to the AFTAN. The color-coded map from blue to red is the amplitude dB. The x-axis represent the time frame in seconds and the y-axis represent the group velocity.

Rayleigh-wave Green's function between stations LSZ and VWP filtered in different frequency bands and stacked for ten months. We approximate the group velocity using FTAN and phase Match Filtering Analysis (MTA) show in Figure 9, and we process a total of 66 dispersion curves from the regional network. We approximate

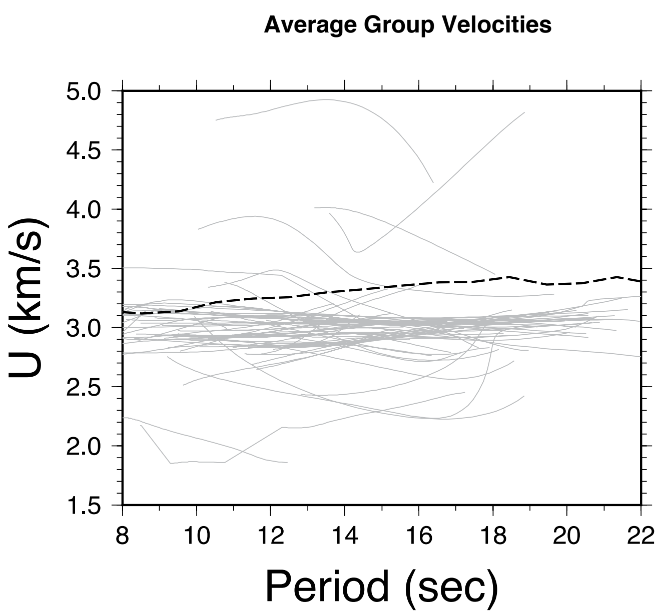

Figure 10. Dash-line is the average group velocities approximate from the many gray dispersions curve. The gray curve represent the number of observe dispersions curve that had been approximated using the AFTAN. The x-axis represent the time frame in seconds and the y-axis represent the group velocity.

the average group velocity from the total of 66 dispersion curves from Figure 10. We will use the dispersion curves in order to approximate the dispersion maps using Barmin (2011) technique.

5. Conclusion

Our preliminary local earthquake locations (Figure 3) appear to be scattered within the caldera, but by acquiring more data for the next two years, we believe our analysis can approximate the hydrothermal system that could target potential drilling sites. In the future, we will process our data for source characterization (i.e., tremor, swarm identification, etc.), and crustal structure determination (receiver functions, tomography, etc.).

References

Árnason, K., and Eysteinsson, H., 2010. Join 1D inversion of TEM and MT data and 3D inversion of MT data in the Hengill area, SW Iceland, *Geothermics*, 39, 13-34.

Ayele, A., Stuart, G., and Kendall, J.M., 2004. Insights into rifting from shear wave splitting and receiver functions: an example from Ethiopia, *Geophysical Journal International*, 157, 354-362.

Barmin, M.P., Ritzwoller M.H., and Levshin A.L., 2001. A fast and reliable method for surface wave tomography, *Pure Appl. Geophys*, 158(8), 1351 - 1375.

Bensen, G.D., Ritzwoller, M.H., Barmin, M.P., Levshin, A.L., and Lin, F., 2007. Processing seismic ambient noise data to obtain reliable broadband surface wave dispersion measurements, *Geophysical Journal International*, 169, 1239-1260.

Bensen, G.D., Ritzwoller, M.H., and Shapiro, N.M., 2008. Broadband ambient noise surface wave tomography across the United States, *Journal of Geophysical Research*, 113, 1-21.

Campillo, M., and Paul, A., 2003. Long-range correlations in the diffuse seismic coda, *Science*, 299, 547-549.

Chouet, B.A., 1996a. Long-period volcano seismicity: Its source and use in eruption forecasting, *Nature*, 380.

Hermann, R.B., and Ammon, C.J., 2004. surf96 from computers programs in seismology, surface waves, receiver functions and crustal structure, version 3.30, Department of Earth and Atmospheric Sciences, Saint Louis University.

Kennet, B.L.N., 1983. Seismic Wave Propagation in Stratified Media, *Cambridge University Press*, Cambridge, England, 1-342.

Langston, C.A., 1976. A body wave inversion of the Koyna, India earthquake of December 10, 1967, and some implications for body wave focal mechanisms, *Journal of Geophysical Research*, 81, 2517-2529.

Langston, C.A., 1981. Source inversion of seismic waveforms: The Koyna, India, earthquakes of 13 September, 1967, *Bulletin of the Seismological Society of America*, 71, 1-24.

Levshin, A.L., Pisarenko, V.F., Pogrebinsky, G.A., 1972. On a frequency-time analysis of oscillations, Ann. Geophys.,28, 211-218.

Lin, F.C., Moschetti, M.P., and Ritzwoller, M.H., 2008. Surface wave tomography of the western United States from ambient seismic noise: Rayleigh and Love wave phase velocity maps, *Geophysical Journal International*, 173, 281-298.

Nicolson, H., Curtis, A., Baptie, B., and Galetti, E., 2012. Seismic interferometry and ambient noise tomography in the British Isles, *Proceeding of the Geologist's Association*, 123, 74-86.

Randall, G.E., Ammon, C.J., and Owens, T.J., 1995. Moment tensor estimation using regional seismograms from a Tibetan Plateau portable network deployment, *Geophysical Research Letters*, 22, 1665-1668.

Ritsema, J., and Lay, T., 1993. Rapid source mechanism determination of large (Mw ≥ 5) earthquakes in the western United States, *Geophysical Research Letters*, 20, 1611-1614.

Silver, P.G., and Chan, W.W., 1991. Shear wave splitting and subcontinental mantle deformation, *Journal Geophysical Research*, 96 B(10), 16429-16454.

Simiyu, S.M., and Keller, G.R., 2001: Geophysical interpretation of the upper crustal structure of the southern Kenya rift, *Geophysical Journal International*, 1245, 234-267.

Simiyu, S.M., 2000: A volcano-seismic approach to geothermal exploration, 5th World Geothermal Congress 2000, Morioka, Japan.

Simiyu, S.M., 2009. Application of micro-seismic methods to geothermal exploration: examples from the Keyna rift, *United Nations University and LaGeo*, 1, 1-27.

Waldhauser, F., 2001: HYPODD—A program to compute double-difference hypocenter locations, *U.S. Geological Survey Open-File Report*.

Waldhauser, F., and Ellsworth, W.L., 2000. A Double-Difference Earthquake Location Algorithm: Method and Application to the Northern Hayward Fault, California, *Bulletin of the Seismological Society of America*, 90.

Wamalwa A. M., 2011. Joint geophysical data analysis for geothermal energy exploration, *ETD Collection for University of Texas, El Paso*. Paper AAI3489993.

Wilson, D., Aster, R., and RISTRA Team, 2003. Imaging crust and upper mantle seismic structure in the southwestern United States using teleseismic receiver functions, *Leading Edge*, 22, 232-237.

Wüstefeld, A., Bikelmann, G., Barruol, G., and Montagner, J.P., 2009. Identifying global seismic anisotropy patterns by correlating shear-wave splitting and surface-wave data, *Physics of the Earth and Planetary Interiors*, 176, 198-212.

Yang, Y., Ritzwoller, M.H., and Jones, C.H., 2011. Crustal structure determined from ambient noise tomography near the magmatic centers of the Coso region, southeastern California, *Geochemistry Geophysics Geosystems*, 12, 1-20.

Yang, Y., Shen, W., and Ritzwoller, M.H., 2011. Surface wave tomography on a large-scale seismic array combining ambient noise and teleseismic earthquake data, *Earthquake Sciences*, 24, 55-64.